3-30-2021

Biological Activity and Solubility of 5-Methoxy-1,4-Benzoquinone Having Bromoheptyl and Bromodecyl Substituents in the n-Octanol/Water System

Siti Mariyah Ulfa
Chemistry Department, Faculty of Science, Universitas Brawijaya, Malang 65145, Indonesia,
ulfa.ms@ub.ac.id

Fath Dwisari
Chemistry Department, Faculty of Science, Universitas Brawijaya, Malang 65145, Indonesia

Laras Pangesti
Chemistry Department, Faculty of Science, Universitas Brawijaya, Malang 65145, Indonesia

Mohammad Farid Rahman
Synthesis and Catalysis of Natural Product Research Group, Faculty of Science, Universitas Brawijaya, Malang 65145, Indonesia

Biological Activity and Solubility of 5-Methoxy-1,4-Benzoquinone Having Bromoheptyl and Bromodecyl Substituents in the n-Octanol/Water System

Biological Activity and Solubility of 5-Methoxy-1,4-Benzoquinone Having Bromoheptyl and Bromodecyl Substituents in the *n*-Octanol/Water System

Siti Mariyah Ulfa[1,2*], Fath Dwisari[1], Laras Pangesti[1], and Mohammad Farid Rahman[1,2]

1. Chemistry Department, Faculty of Science, Universitas Brawijaya, Malang 65145, Indonesia
2. Synthesis and Catalysis of Natural Product Research Group, Faculty of Science,
Universitas Brawijaya, Malang 65145, Indonesia

e-mail: ulfa.ms@ub.ac.id

Abstract

The biological activity and solubility of compounds are influenced by its chemical structure. These properties can be improved by substituting alkyl, alkoxy, and/or haloalkane in the parent skeleton. In this research, the synthesis of 3-(7-bromoheptyl)-2-methyl-5-methoxy-1,4-benzoquinone (**3a**) and 3-(10-bromodecyl)-2-methyl-5-methoxy-1,4-benzoquinone (**3b**) was achieved through the decarboxylation reaction. The solubility and biological activity of **3a** and **3b** were compared with that of thymoquinone (**TQ**), which acts as an anti-inflammatory agent. Compounds **3a** and **3b** were successfully synthesized and analyzed using Fourier Transform Infra-Red (FTIR) and Nuclear Magnetic Resonance (NMR). The FTIR spectrum showed the increasing intensity of C-H sp^3 and the absorption of C-Br because of the presence of the bromoheptyl and bromodecyl substituents. ^{1}H-NMR showed the prominent chemical shift of olefinic methylene at δ 1.29–3.40 ppm. The solubility test showed the differences in the partition coefficient (log *P*) of **3a** and **3b** in the *n*-octanol/water system. The log *P* values of **3a** and **3b** are higher than those of **TQ**, indicating that methoxy, bromoheptyl, and bromodecyl support the increase in solubility. Biological activity test using the in silico approach showed that **3a** and **3b** have a higher tendency to bind with the translocator protein (TSPO) macromolecule than the phosphatase and tensin homolog (PTEN) macromolecule. The binding interactions of TSPO-**3a** and TSPO-**3b**, similar to that of TSPO-**TQ**, showed that both synthesized compounds have comparable activity. The binding energy of TSPO-**3a** is lower than that of TSPO-**3b**, indicating that **3a** has a higher activity for anti-inflammatory drug candidates than **3b**.

Keywords: 1,4-benzoquinone, bromoalkylation, partition coefficient, thymoquinone, lipophilicity

Introduction

Naturally occurring quinones, such as 2-isopropyl-5-methyl-1,4-benzoquinone, also known as thymoquinone (**TQ**), are an active constituent of *Nigella sativa* seed oil [1]. The therapeutic effect of *N. sativa* seed oil with TQ on the treatment of several chronic diseases, such as cancer and inflammatory disorders, has been investigated [2,3]. However, pharmacokinetic studies of TQ by oral administration in an animal model showed rapid elimination and relatively slow absorption [4]. To improve the bioavailability and biological activity of quinone-based drugs, structure modification by inserting polar and/or nonpolar functional groups, such as methoxy and bromoalkyl substituents, has become a promising and interesting subject.

Quinone-containing alkylating agents, such as mitomycin C, also known as "bioreductive alkylating drugs," refer to drugs with an electrophilic substituent to bind covalently to cellular macromolecules [5]. Novel quinone derivatives, including alkylated cationic **TQ**, such as SkQT1 and SkQ1, have also been reported [6]. SkQT1 and SkQ1 are potential antioxidants that target mitochondria because the inner membrane of mitochondria is negatively charged. Recently, the synthesis of benzoquinone having bromoalkyl substituents, such as 3-(10-bromodecyl)-5-isopropyl-2-methyl-1,4-benzoquinone [7], 5-(7-bromoheptyl)-2,3-dimethyl-1,4-benzoquinone [8], 2-(5-bromoamyl)-3,5-dimethyl-1,4-benzoquinone [9], and phosphonium-1,4-benzoquinone derivatives, have been reported [10] (**Figure 1**). In silico analysis of these compounds showed that the bromoheptyl (C7) and bromodesyl (C10) substituents effectively increased solubility in the *n*-octanol/water system. By contrast, methoxy (–OMe) attached to 5-methyl-1,4-benzoquinone without bromoalkyl substituent resulted in decreased solubility [11]. In this research, the synthesis of 1,4-benzoquinone derivatives with methoxy and bromoalkyl substituents is proposed to increase the biological activity and solubility compounds.
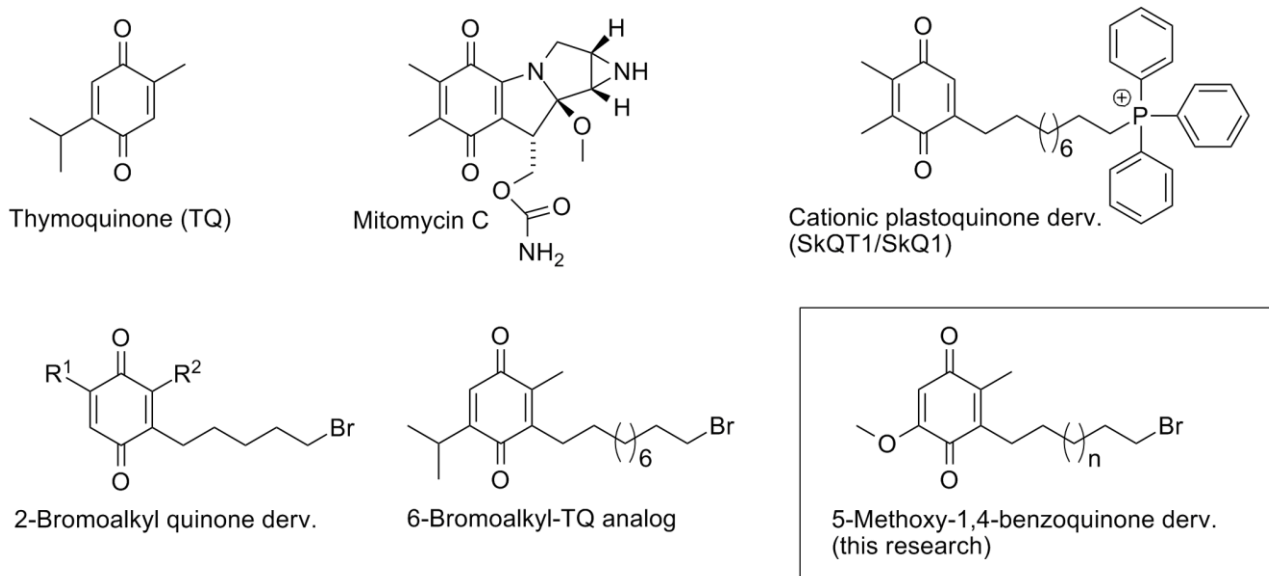
Figure 1. Examples of Quinone-based Derivatives

First, the solubility of drug candidate compounds is considered. Then, the biological activity of drug candidate compounds is evaluated using in silico molecular docking between macromolecule (proteins or enzymes) and ligand [12]. The binding of compounds with a specific receptor is calculated for the free energies (ΔG^o) of protein–ligand complexes, the inhibitory constant (Ki), and the half-maximal inhibitory concentration (IC_{50}). The data of many drug candidates have been analyzed on the basis of the Ki value instead of the IC_{50} value because Ki is an intrinsic and thermodynamic quantity that depends on the enzyme and inhibitor. By contrast, the IC_{50} value depends on concentrations of the target macromolecule, inhibitor, and ligand, along with other experimental conditions [13]. The target macromolecule for in silico design is close to human disease and binds to a small molecule to yield a function [14]. In this research, we introduced the translocator protein (TSPO) and phosphatase and tensin homolog (PTEN). TSPO is an 18 kDa transmembrane protein primarily found in the outer mitochondrial membrane, which mainly suppresses inflammatory disorders. TSPO is a prospective protein model because its interaction with the endogenous and exogenous ligands, i.e., having the methoxy substituent, has rarely been reported. The families of heterocyclic molecules with at least one nitrogen and/or carbonyl group (C=O) responds to TSPO [15]. Another macromolecule is PTEN, which induces the apoptosis of cancer cells [16].

In summary, we highlighted the synthesis of 3-(7-bromoheptyl)-2-methyl-5-methoxy-1,4-benzoquinone (**3a**) and 3-(10-bromodecyl)-2-methyl-5-methoxy-1,4-benzoquinone (**3b**). Solubility was evaluated using the shake-flask method. Biological activity was evaluated

using in silico molecular docking, with TSPO and PTEN as macromolecules.

Materials and Methods

Materials. 2-Methyl-1,4-benzoquinone (**1**) was obtained from Sigma-Aldrich (Singapore) and directly used for the synthesis of 2-methyl-5-methoxy-1,4-benzoquinone (**2**). Other chemicals, such as 8-bromooctanoic acid ($C_8H_{15}BrO_2$), 11-bromoundecanoic acid ($C_{11}H_{21}BrO_2$), and ammonium persulfate (($NH_4)_2S_2O_4$), were also purchased from Sigma-Aldrich (Singapore). Silver nitrate ($AgNO_3$) and sodium sulfate (Na_2SO_4) were obtained from Merck (Singapore) and used as drying agents. The solvents acetonitrile, ethyl acetate, diethyl ether, and *n*-hexane supplied by Merck (Singapore) were of analytical grade.

Instrumentations. The UV–Visible Shimadzu 1600, FTIR Shimadzu 8400S, HPLC Shimadzu LC-20AD Prominence with FID detector, and NMR spectroscopy JEOL ECS400 were used in this research.

Synthesis of the 5-methoxy-1,4-benzoquinone derivatives 3a and 3b. 2-Methyl-5-methoxy-1,4-benzoquinone (**2**) was prepared by substitution of methoxy into 2-methyl-1,4-benzoquinone (**1**) using methanol as a nucleophile (**Scheme 1**) according to previous research [11]. Compound **2** was obtained as a yellow needle crystal and directly used for the synthesis of **3a** and **3b**. The synthesis of **3a** and **3b** was achieved through the decarboxylation reaction as follows [8]: Compound **2** (2.0 mmol, 304 mg) was combined with 8-bromooctanoic acid (2.1 mmol, 468 mg) to synthesize **3a** or 11-bromoundecanoic acid (2.1 mmol, 556 mg) to

---

synthesize **3b**. AgNO₃ (1.0 mmol, 169 mg) and acetonitrile/H₂O (2:1) were added and stirred at a temperature of 80 °C. Afterward, (NH₄)₂S₂O₈ (2 mmol, 456 mg) in 3 mL H₂O was added dropwise, stirred for 60–90 min, and maintained at temperatures of 70 °C to 80 °C. The obtained mixture was extracted with diethyl ether. The organic phase was separated and dried over Na₂SO₄. The excess solvent was evaporated to obtain the brownish red liquid product. The crude product was purified by SiO₂ column chromatography using *n*-hexane/chloroform (6:4 ratio (v/v)). **3a** and **3b** were characterized using FTIR Shimadzu 8400S, UV–Visible Shimadzu 1600, and ¹H-NMR 400 MHz in CDCl₃ and TMS as the internal standard. Physical properties of the synthesis compounds: 3-(7-bromoheptyl)-2-methyl-5-methoxy-1,4-benzoquinone (**3a**): yellow oil (20 mg; 1.41%). Thin-layer chromatography (TLC) analysis using *n*-hexane/ethyl acetate (7:3) yielded Rf = 0.62; UV–Vis analysis yielded λₘₐₓ = 264 nm. FTIR analysis (cm⁻¹): 2,925 (C-H sp³), 1,728 (C=O), 1,649 (C=C), 1,460 (CH₂), 1,274 (C-O), 565 (C-Br); ¹H-NMR (400 MHz, CDCl₃) δ 8.09 (s, 1H, H-1), 3.91 (s, 3H, –OCH₃), 3.40 (t, 2H, J = 6.4 Hz, H-3), 2.41 (t, 2H, J = 7.1 Hz, H-4), 2.02 (s, 3H, H-5), 1.85 (m, 2H, J = 6.4, 7.1 Hz, H-6), 1.56–1.28 (d, 8H, J = 6.4, 7.1 Hz, H-7). 3-(10-bromodecyl)-2-methyl-5-methoxy-1,4-benzoquinone (**3b**): yellow oil (10 mg; 0.76%). TLC analysis using *n*-hexane/ethyl acetate (7:3) yielded Rf = 0.58; UV–Vis analysis yielded λₘₐₓ = 260 nm. FTIR analysis (cm⁻¹): 2,854 (C-H sp³), 1,647 (C=O), 1,460 (C=C), 1,226 (C-O), 636 (C-Br); ¹H-NMR (400 MHz, CDCl₃) δ 8.09 (s, 1H, H-1), 3.91 (s, 3H, –OCH₃), 3.40 (t, 2H, J = 6.4 Hz, H-3), 2.41 (t, 2H, J = 6.8 Hz, H-4), 2.02 (s, 3H, H-5), 1.85 (m, 2H, J = 6.4 Hz, H-6), 1.38–1.28 (d, 14H, J = 6.4 Hz, H-7).

Solubility test of 3a and 3b in the *n*-octanol/water system. Before the solubility test, the hydrophobic and hydrophilic phases were prepared according to the following procedure [17]: A phosphate buffer solution (pH 7.4) was prepared by mixing 67 mL NaH₂PO₄·H₂O (0.1 M) with 330 mL Na₂HPO₄ (0.1 M). This solution was designated as the water system. The water system was saturated with *n*-octanol to obtain the hydrophilic phase. Meanwhile, the hydrophobic phase was prepared by saturating *n*-octanol with the water system. Both solutions were mixed for at least 24 h and then separated. Compounds **3a**, **3b**, and **TQ** were dissolved in *n*-octanol (10 mM). Then, *n*-octanol containing the compounds was mixed with water in 3:7 (v/v) partition for 1 h at room temperature using an orbital shaker. Afterward, *n*-octanol and water were separated. HPLC analysis of water and *n*-octanol was performed by injecting 2 μL of each partition with 0.5 mL/min flow rate at 37 °C. The distribution of each compound in *n*-octanol and water was calculated using Eq. 1, where C₍octanol₎ and C₍water₎ are the total drug concentration in *n*-octanol and water. The total drug concentration was

derived from the peak areas of **3a** and **3b** in *n*-octanol (Aₒ) and water (A𝓌) divided by the volumes of the *n*-octanol (Vₒ) and water (V𝓌) partitions.

$$\text{Log } P = \log \frac{C_{\text{octanol}}}{C_{\text{water}}} = \log \frac{A_o/V_o}{A_w/V_w} \quad (1)$$

Biological evaluation of 3a and 3b using the in silico approach. The biological evaluation of **3a** and **3b** was conducted using AutoDock4. The ligand structures of **3a**, **3b**, and **TQ** were optimized using HyperChem and saved in.pdb format. The TSPO and PTEN macromolecule models were downloaded from www.rcsb.org and saved in.pdb format. Both water and external ligands were removed from the macromolecules. The docking process consists of two main steps, namely, running AutoGrid (format conversion into.gpf) and running AutoDock (format conversion into.dpf). The AutoDock parameter was used to calculate the van der Waals and electrostatic terms. Docking simulations were performed using the Lamarckian genetic algorithm. The grid boxes for the macromolecules used in this research were designed using AutoGrid4, with TSPO box dimensions for **3a**, **3b**, and **TQ** of x = 32.778, y = −17.093, and z = 69.101 and PTEN box dimensions for **3a**, **3b**, and **TQ** of x = 268.883, y = 19.827, and z = 47.339. AutoDock4 was run to determine the minimum energy for each bond. The results of binding interactions (Ki), minimum energy, and amino acid and ligand interactions were analyzed using the Discovery Studio Visualizer [8].

Results and Discussion

The synthesis of **3a** and **3b** was achieved through the decarboxylation reaction using 8-bromooctanoic acid and 11-bromoundecanoic acid. The synthesis routes are shown in **Scheme 1**. Compounds **3a** and **3b** were obtained as brownish oil with 1.41% and 0.76% yields, respectively. Compared with that of a similar reaction, the product yields of **3a** and **3b** through the decarboxylation reaction were relatively low. The presence of methoxy (–OMe) at the *meta*-position probably suppressed the alkylation reaction [18]. The synthesis strategy should be improved to increase the reaction yield by prolonging the reaction time and/or increasing the reaction temperature.

TLC analysis showed that **3a** and **3b** have a similar retardation factor (Rf). Compared with 2-methyl-5-methoxy-1,4-benzoquinone (**2**), both alkylation products **3a** and **3b** showed a larger Rf, which indicates that the insertion of the alkyl group into 1,4-benzoquinone decreased the polarity of the compound. Additional analysis using UV–Vis showed that the introduction of alkyl increased the wavelengths of **3a** and **3b**, resulting in a redshift. FTIR analysis of **3a**, **3b**, and **2** (**Figure 2**)
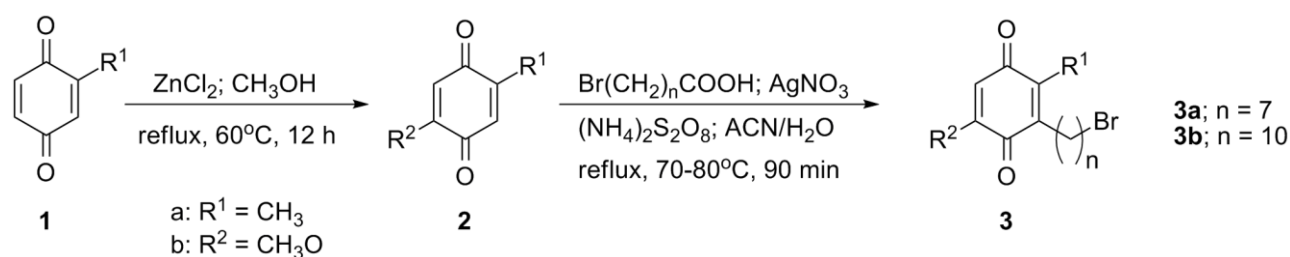
Scheme 1. Synthesis Overview
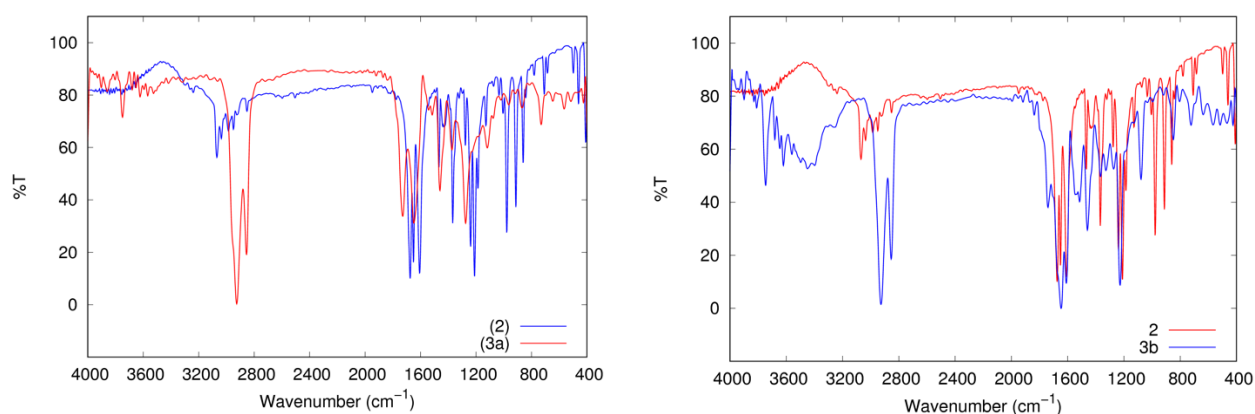
Figure 2. FTIR spectra of 3a (left) and 3b (right)

showed a significant difference between these compounds. The increase in the intensity of the C-H sp^3 peak at 2,924 cm^{-1} (**3a**) and 2,854 cm^{-1} (**3b**) was due to the substitution of alkyl in benzoquinone. The new peaks at 646 and 636 cm^{-1} corresponded to C-Br in compounds **3a** and **3b**, respectively. The overall analysis indicated that the addition of alkyl substitution to the synthesis process has been successful [8].

The structures of the quinone skeletons of **3a** and **3b** are similar; hence, only compound **3a** is discussed in detail as follows (see **Table 1**, **Figure 3**): The presence of a singlet peak at δ 8.09 ppm (1H, s) indicates that one proton attached to the benzoquinone ring. From this pattern, it is assumed that the alkylation reaction only replaces one proton at C-3 or C-6. Further analysis showed the proton appears in the high-field region at δ 0.85–2.41 ppm, which indicates an aliphatic proton. The peak at δ 2.41 ppm (2H, br) corresponds to the methylene proton that directly attached to the quinone ring with the sequence Ar–**CH₂**–R, and the peak at δ 1.85 ppm (2H, m) corresponds to the methylene proton that directly attached to the quinone ring with the sequence R–**CH₂**–R. The other multiplet at 1.56–1.28 (8H, m) corresponds to aliphatic methylene in saturated alkane. The terminal methylene, which is directly attached to bromine R–**CH₂**–Br, is observed at δ 3.40 ppm (t, 2H, J = 6.4 Hz). The methyl proton shifted to 1.84 ppm (3H, s), and methoxy was detected as a sharp

singlet peak at 1.56 ppm (3H, s). Some impurities at δ 0.88 ppm from silicon grease were also observed. The results of NMR analysis are consistent with previously reported data [7,8].

The solubility test, calculated as log P, was performed using the shake-flask method with *n*-octanol and water as partitioning system [17]. The distributions of **3a** and **3b** in the *n*-octanol/water system were determined by HPLC. *n*-Octanol is generally used as a model solvent to understand the partitioning of compounds from water into lipid membranes [19]. The log P values of **3a** and **3b** are shown in **Table 2**. The results showed a slightly higher log P value for **3a** than that for **TQ**. Compound **3b** has the highest log P value among the other compounds; thus, the order of solubility is **3b** > **3a** > **TQ**. The comparison of the log P calculation using the ALOGPS 2.1 program [20] and the in vitro analysis (HPLC method) indicated that the order of solubility is the same. Thus, the increase in alkyl substituent concomitantly increases the solubility of the compound in the *n*-octanol phase. These results follow Lipinski's rule of five, i.e., the log P value for the oral administration of drug candidates is not more than 5 [21]. Two main factors can rationalize the effect of alkyl substituent on the solubility of the compounds in the *n*-octanol/water system, i.e., the molecular polarity and the tendency for hydrogen bonding with the solvents [19].
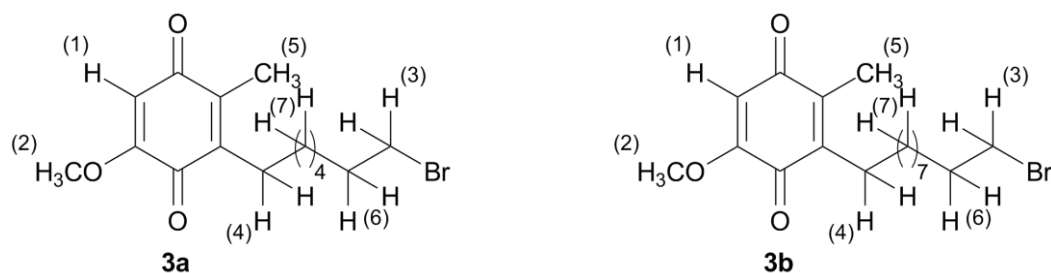
Figure 3. Structure Determination of Compounds 3a and 3b

Table 1. ^{1}H-NMR Spectral Data of Compounds 3a and 3b

Position	3a δ_H (*J* in Hz)	3b δ_H (*J* in Hz)
1	8.09 (s, 1H)	8.09 (s, 1H)
2	3.91 (s, 3H, -OCH$_3$)	3.91 (s, 3H, -OCH$_3$)
3	3.40 (t, 2H, *J* = 6.4)	3.51 (t, 2H, *J* = 6.4)
4	2.41 (t, 2H, *J* = 7.1)	2.41 (t, 2H, *J* = 7.1)
5	2.02 (s, 3H)	2.43 (s, 3H)
6	1.85 (m, 2H, *J* = 6.4, 7.1)	1.85 (m, 2H, *J* = 6.4, 7.1)
7	1.56–1.28 (m, 8H *J* = 7.1, 6.4)	1.29 (m, 14H, *J* = 7.1, 6.4)

Table 2. Solubility Test

Compound	log *P* In vitro[a]	log *P* Prediction[b]
3a	2.22	3.64
3b	3.03	5.00
TQ	2.17	2.80

a) HPLC analysis
b) Predicted using the ALOGPS 2.1 program

Table 3. In silico data of 3a, 3b, and TQ with TSPO and PTEN macromolecule models

| Macromolecules	Ligand	ΔG^o (kcal/mol)	Ki (µM)	IC$_{50}$ (µg/mL)
TSPO	**3a**	−5.52	92.16	60.68
	3b	−5.21	157.92	117.40
	TQ	−5.88	49.02	16.10
PTEN	**3a**	−5.07	214.29	141.10
	3b	−4.59	434.77	323.22
	TQ	−4.77	335.29	110.11

The activities of **3a**, **3b**, and **TQ** were analyzed using in silico molecular docking. The binding interactions of **3a**, **3b**, and **TQ** with TSPO and PTEN macromolecule models were also evaluated. The data collected from in silico molecular docking are depicted in **Table 3**. The binding energies (ΔG^o) of **3a**, **3b**, and **TQ** with TSPO varied from −5.21 kcal/mol to −5.88 kcal/mol. However, the binding energies (ΔG^o) of **3a**, **3b**, and **TQ** with PTEN were slightly higher than those with TSPO.

All three compounds showed a tendency to inhibit the macromolecule models because ΔG^o has a negative value. The Ki values (**Table 3**) of **3a**, **3b**, and **TQ** show

that these compounds have a more robust interaction with TSPO than with PTEN. Compound **3a** has a lower Ki value than **3b** by 1.71-fold, and **TQ** has a lower Ki value than **3a** by 1.88-fold. The order of inhibition toward the TSPO ligand is **TQ** > **3a** > **3b**. Although compounds **3a** and **3b** have lower binding energies than **TQ**, the presence of the 7-bromoheptyl substituent in **3a** is more favorable than that of 10-bromodecyl in **3b**. Compound **3b** has a longer alkyl substituent than **3a**; however, it does not ensure better inhibition toward the target macromolecules. The longer alkyl substituent increased the log *P* (**Table 2**); however, it might suppress the activity [22]. The predicted IC$_{50}$ values of **3a** and **3b** supported the order of the Ki value. In summary, compound **3a** exhibited better properties as a drug candidate than **3b** for interaction with the TSPO macromolecules.

Confirmation of the substrate-binding residues between ligands **3a** and **3b** with TSPO and PTEN is shown in **Figure 4**. The binding interaction of the amino acid residue on PTEN-**3a** and PTEN-**3b** is less than that on TSPO-**3a** and TSPO-**3b**. This result supports the prediction that the activities of **3a** and **3b** with PTEN are lower than that with TSPO. Further analysis revealed the hydrogen bonding and van der Waals interaction between enzyme and substrate, which are the critical relationships between ligands and macromolecules. The aromatic quinone ring on **3a** has actively interacted with residue TRP135 with the backbone indole group (*N*-aromatic amino acid), indicating the van der Waals interaction. Moreover, the carbonyl from quinone is strongly hydrogen bonded to the peptide chain of the amino group of TRP50. The hydrophobic nature of

TSPO-3a

TSPO-3b

PTEN-3a

PTEN-3b
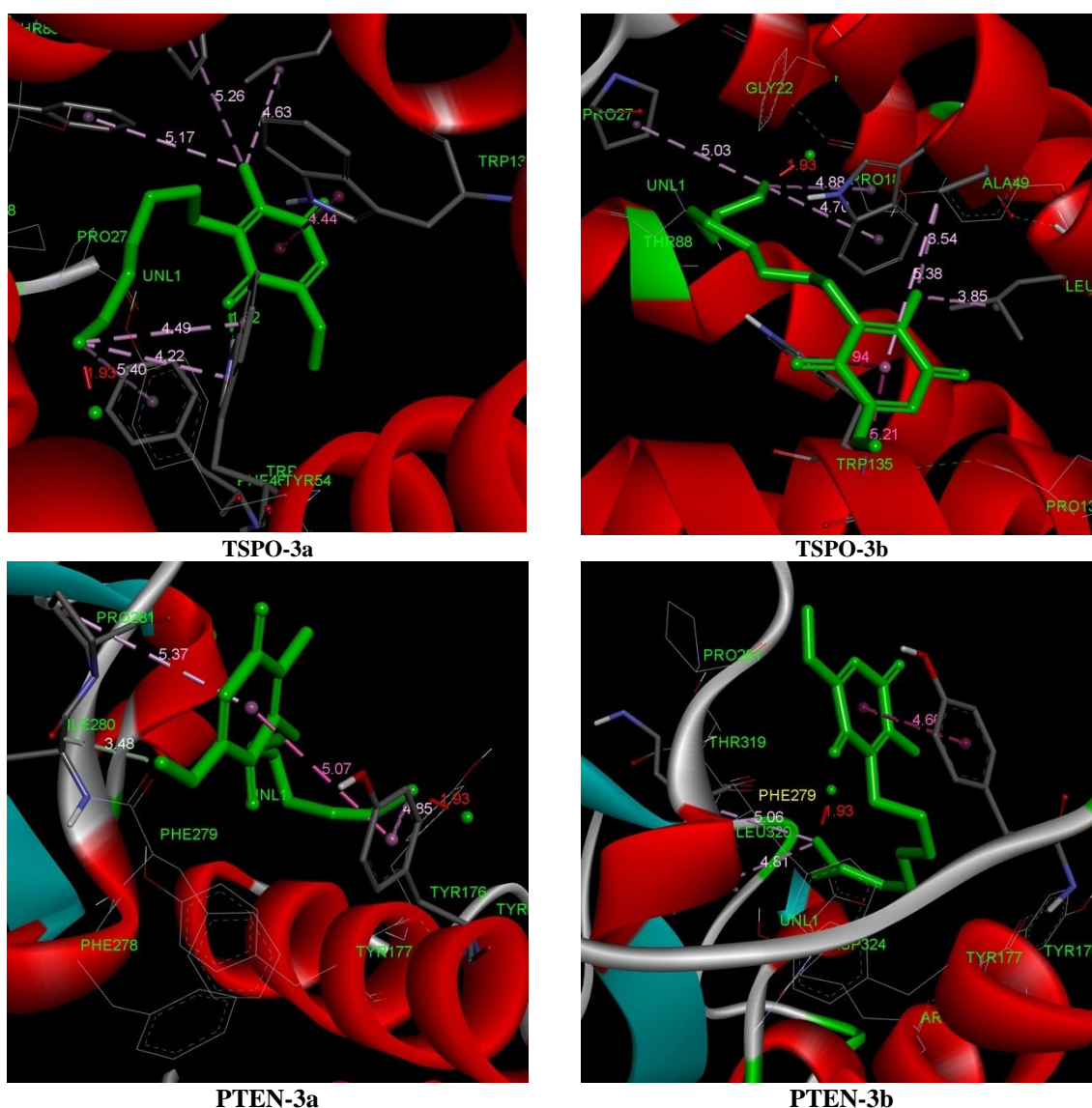
Figure 4. Molecular Visualization of the Binding Interaction between Ligand 3a and 3b with TSPO and PTEN

benzyl residues from PHE46 and PHE92 strongly interacted with the alkyl group from **3a**. However, compared with the interaction of TSPO-**3b**, no hydrogen bonding occurred between carbonyl and amino acid residues from TRP50. The significant interaction is the van der Waals interaction between alkyl and hydrophobic residues, such as TRP135, ILE134, and ALA49. The interaction of quinone with TRP135 in TSPO-**3b** has a longer distance (5.94 Å) than TSPO-**3a** (4.44 Å). The hydrogen bonding in TSPO-**3a** with TRP50 has a relatively close range, i.e.,, 1.52 Å. Thus, we inferred that these residues were vital to substrate bonding because of their location within the hydrogen bonding distance (<3 Å) to the substrate [23]. The overall result indicated that the addition of an alkyl residue, i.e., 7-bromoalkyl, to the quinone ring partially supports solubility and improves the activity with TSPO as target macromolecule.

Conclusion

The synthesis of 5-methoxy-1,4-benzoquinone having bromoheptyl and bromodecyl substituents **3a** and **3b** was achieved through the decarboxylation reaction. The evaluation of its solubility indicated that the bromoalkyl substituent increased the solubility of compounds in *n*-octanol. The activities of **3a** and **3b** toward the TSPO macromolecule indicated that TSPO-**3a** had a lower binding energy and IC$_{50}$ than TSPO-**3b**. The analysis of the substrate-binding residue showed that TSPO-**3a** has a stronger hydrogen bond with the amino acid residue than TSPO-**3b**, indicating that TSPO-**3a** has better activity than TSPO-**3b**. The binding of **3a** and **3b** toward PTEN showed a lower interaction than that toward TSPO. The addition of bromoheptyl and bromodecyl to the 1,4-benzoquinone ring promotes the increase in solubility. Thus, the binding of the compound

with TSPO indicated that **3a** is a promising compound for anti-inflammatory drug candidates.

Acknowledgment

References

[1] Amin, B., Hosseinzadeh, H. 2015. Black Cumin (*Nigella sativa*) and Its Active Constituent, Thymoquinone: An Overview on the Analgesic and Anti-inflammatory Effects. Planta Med. 82: 8–16, https://doi.org/10.1055/s-0035-1557838.

[2] Rashidmayvan, M., Mohammadshahi, M., Seyedian, S.S., Haghighizadeh, M.H. 2019. The Effect of *Nigella sativa* Oil on Serum Levels of Inflammatory Markers, Liver Enzymes, Lipid Profile, Insulin and Fasting Blood Sugar in Patients with Non-alcoholic Fatty Liver. J. Diabetes. Metab. Disord. 18: 453–9, https://doi.org/10.1007/s40200-019-00439-6.

[3] Johnson-Ajinwo, O.R., Ullah, I., Mbye, H., Richardson, A., Horrocks, P., Li, W-W. 2018. The Synthesis and Evaluation of Thymoquinone Analogues As Anti-ovarian Cancer and Antimalarial Agents. Bioorg. Med. Chem. Lett. 28: 1219-1222. https://doi.org/10.1016/j.bmcl.2018.02.051.

[4] Alkhrafy, K., Ahmad, A., Khan, R., Al-Shagha, W. 2015. Pharmacokinetic Plasma Behaviours of Intravenous and Oral Bioavailability of Thymoquinone in Rabbit Model. Eur. J. Drug. Metab. Pharmacokinet. 40: 319-323. https://doi.org/10.1007/s13318-014-0207-8.

[5] Lin, J., Cosby, L.A., Sartorelli, C. 1972. Potential Bioreductive Alkylating Agents. 1. Benzoquinone Derivatives. J. Med. Chem. 15: 1247-1252.

[6] Antonenko, Y.N., Avetisyan, A.V., Bakeeva, L.E., Chernyak, B.V., Chertkov, V.A., Domnina, L.V., *et al.* 2008. Mitochondria-targeted Plastoquinone Derivatives as Tools to Interrupt Execution of the Aging Program. 1. Cationic Plastoquinone Derivatives: Synthesis and In Vitro Studies. Biochemistry (Mosc). 73: 1273-1287. https://doi.org/10.1134/S0006297908120018.

[7] Setyatama, N.E., Ulfa, S.M., Okamoto, H. 2018. Synthesis and Activity Analysis of 3-(10-Bromodecyl)-5-isopropyl-2-methyl-1,4-benzoquinone: In-silico Approach. Proceedings of the 1st International Conference in One Health (ICOH 2017), Malang, Indonesia: Atlantis Press. https://doi.org/10.2991/icoh-17.2018.24.

[8] Ulfa, S.M., Sholikhah, S., Utomo, E.P. 2017. Synthesis of Thymoquinone Derivatives and Its Activity Analysis: In-silico Approach. AIP Conference Proceedings. 020102. https://doi.org/10.1063/1.4978175.

[9] Ulfa, S.M., Dwisari, F., Sally, A.C., Rahman, M.F. 2020. Effect of Methyl Substituent on the Solubility of 1,4-Benzoquinone Derivatives in *n*-Octanol/water System. J. Kim. Sains. Apl. 23: 142–6. https://doi.org/10.14710/jksa.23.5.142-146.

[10] Furoida, A., Ulfa, S.M. 2019. Synthesis of 3-(7-Triphenylphosphonioheptyl)-2,6-dimethyl-1,4-benzoquinone) and The Activity Test Toward Glycogen Phosphorylase Enzyme: *In silico* Approach. IOP Conf Ser: Mater Sci Eng 546: 062008. https://doi.org/10.1088/1757-899X/546/6/062008.

[11] Dwisari, F., Srihardyastutie, A., Ulfa, S.M. 2019. Synthesis of 2-Methyl-5-methoxy-1,4-benzoquinone and In-silico Activity Profiling Toward Cytochrome P450-3A4. IOP Conf Ser: Mater Sci Eng. 546: 062005. https://doi.org/10.1088/1757-899X/546/6/062005.

[12] Ekins, S., Mestres, J., Testa, B. 2007. In Silico Pharmacology for Drug Discovery: Methods for Virtual Ligand Screening and Profiling. Br. J. Pharmacol. 152: 9-20. https://doi.org/10.1038/sj.bjp.0707305.

[13] Cer, R.Z., Mudunuri, U., Stephens, R., Lebeda, F.J. 2009. IC50-to-Ki: A Web-based Tool for Converting IC50 to Ki Values for Inhibitors of Enzyme Activity and Ligand Binding. Nucleic Acids Res. 37: 441-445. https://doi.org/10.1093/nar/gkp253.

[14] Anderson, A.C. 2003. The Process of Structure-Based Drug Design. Chemistry & Biology. 10: 787–97. https://doi.org/10.1016/j.chembiol.2003.09.002.

[15] Lacapere, J-J., Duma, L., Finet, S., Kassiou, M., Papadopoulos, V. 2019. Insight Into the Structural Features of TSPO: Implications for Drug Development. Trends Pharmacol. Sci. S0165614719302652. https://doi.org/10.1016/j.tips.2019.11.005.

[16] Arafa, E-SA., Zhu, Q., Shah, Z.I., Wani, G., Barakat, B.M., Racoma, I., *et al.* 2011. Thymoquinone Up-regulates PTEN Expression and Induces Apoptosis in Doxorubicin-resistant Human Breast Cancer Cells. Mutat. Res. 706: 28-35. https://doi.org/10.1016/j.mrfmmm.2010.10.007.

[17] Andrés, A., Rosés, M., Ràfols, C., Bosch, E., Espinosa, S., Segarra, V., et al. 2015. Setup and Validation of Shake-flask Procedures for the Determination of Partition Coefficients (logD) from Low Drug Amounts. Eur. J. Pharm. Sci. 76: 181-191. https://doi.org/10.1016/j.ejps.2015.05.008.

[18] Xu, X-L., Li, Z. 2017. Catalytic Electrophilic Alkylation of *p*-Quinones through a Redox Chain Reaction. Angew. Chem. Int. Ed. 56: 8196–200. https://doi.org/10.1002/anie.201702885.

[19] Rich, P.R., Harper, R. 1990. Partition Coefficients of Quinones and Hydroquinones and Their Relation to Biochemical Reactivity. FEBS Lett. 269: 139-144. https://doi.org/10.1016/0014-5793(90)81139-F.

[20] Tetko, I.V., Tanchuk, V.Yu. 2002. Application of Associative Neural Networks for Prediction of Lipophilicity in ALOGPS 2.1 Program. J. Chem. Inf. Comput. Sci. 42: 1136-1145. https://doi.org/10.1021/ci025515j.

[21] Lipinski. C.A., Lombardo, F., Dominy, B.W., Feeney, P.J. 2012. Experimental and Computational Approaches to Estimate Solubility and Permeability in Drug Discovery and Development Settings. Adv. Drug Deliv. Rev. 64: 4-17.

[22] Iitsuka, Y., Tanaka, Y., Hosono-Fukao, T., Hosono, T., Seki, T., Ariga, T. 2009. Relationship Between Lipophilicity and Inhibitory Activity Against Cancer Cell Growth of Nine Kinds of Alk(en)yl Trisulfides With Different Side Chains. Oncol. Res. 18: 575–82. https://doi.org/10.3727/096504010X12767359113965.

[23] Yan, E.C.Y., Kazmi, M.A., Ganim, Z., Hou, J-M., Pan, D., Chang, B.S.W., *et al.* 2003. Retinal counterion switch in the photoactivation of the G protein-coupled receptor rhodopsin. Proc. Natl. Acad. Sci. 100: 9262-92677. https://doi.org/10.1073/pnas.1531970100.